Structural fingerprints in the reflectance anisotropy of AlInP(001)

I. A. Ruiz Alvarado,[1] M. A. Zare Pour,[2] T. Hannappel,[2] and W. G. Schmidt[1]
[1]*Lehrstuhl für Theoretische Materialphysik, Universität Paderborn, 33095 Paderborn, Germany*
[2]*Grundlagen von Energiematerialien, Institut für Physik, Technische Universität Ilmenau, 98693 Ilmenau, Germany*

(Received 23 May 2023; accepted 7 July 2023; published 18 July 2023)

The surface optical anisotropy of AlInP(001) surfaces is studied from both experiment and theory. The comparison of the data measured on epitaxially grown $Al_{0.52}In_{0.48}P(001)$ epilayers lattice matched to GaAs with spectra calculated for energetically favored AlInP(001) surface structures suggests that the surface is covered with a monolayer of buckled phosphorus dimers, where half of the phosphorus atoms are hydrogen saturated. While the optical anisotropies for photon energies below about 3 eV provide clear fingerprints for the structure of the outermost surface atomic layer, the spectral features at higher energies provide insight into the near surface bulk ordering of AlInP. In particular optical anisotropies at the AlInP critical point energies are found to be related to the CuPt ordering in the material.

DOI: 10.1103/PhysRevB.108.045410

I. INTRODUCTION

The $Al_xIn_{1-x}P$ (AlInP) material system is frequently used as window layer in solar cells, due to its favorable combination of chemical stability, sufficiently wide band gap, and high quality heteroepitaxial interfaces with many absorbers [1]. The Fermi level pinning due to AlInP surface states is highly relevant for the device performance [2]. This holds also for the usage of AlInP as intermediate layer in electronic devices [3]. However, little is known about the atomic structure and electronic properties of AlInP surfaces. It has been noted that different growth conditions lead to different degrees of CuPt ordering in the bulk material [4,5], i.e., alternating group III layers perpendicular to the $[\bar{1}11]$ or $[1\bar{1}1]$ directions. This is likely to be related to the formation of surface dimers, which induce strain in the material [6]. Indeed, the formation of a complete layer of phosphorus dimers (see 2D-2H structures in Fig. 1) was recently predicted for preparation conditions typical for metal organic vapor phase epitaxy (MOVPE) growth [8]. Depending on the surface preparation conditions, however, further clean and hydrogen-adsorbed AlInP(001) surfaces are expected to be stable. The structures most prominent in the surface phase diagrams obtained from *ab initio* thermodynamics [7,8] are compiled in Fig. 1.

Reflectance anisotropy spectroscopy (RAS), also known as reflectance difference spectroscopy [9], is a powerful tool to characterize surfaces at the atomic level: the measurement of the polarization-dependent reflectivity provides insight in the surface structural and electronic properties [10–13]. RAS is nondestructive and can be used in a wide range of environments. It has been used already to monitor the growth of ternary IIIV surfaces and heterostructures [14–17]. In particular, Zorn *et al.* [18] explored the relationship between growth temperature and the ordering of GaInP with RAS. With increasing temperature the (2×1) surface, related to a high degree of order, transitions to the (2×4) surface associated with less ordering. This was corroborated by Kramer *et al.* [19], demonstrating that RAS cannot only be used to obtain insight in the surface anisotropies, but also on the type of bulk ordering. The understanding and interpretation of the RAS spectra, however, requires numerical simulations. There are RAS calculations for binary III-V surfaces; see, e.g., Refs. [20–24]. However, they are not necessarily suitable to explain spectra of ternary systems, where surface-induced bulk ordering processes may lead to additional optical anisotropies.

This motivates the present study. On the one hand, we aim at a better general understanding of the surface optical anisotropy of ternary alloys. We are interested in the sensitivity of RAS with respect to specific surface structural motifs and with respect to ordering effects in near surface layers. On the other hand, we want to employ RAS specifically for a better understanding of the MOVPE-grown AlInP(001) surface. Therefore, we compare data measured for epitaxially grown $Al_{0.52}In_{0.48}P(001)$ epilayers with spectra simulated for the energetically most relevant $Al_{0.5}In_{0.5}P$ (001) surface structures shown in Fig. 1.

II. METHODOLOGY

Thin $Al_{0.52}In_{0.48}P(001)$ layers were prepared in a horizontal MOVPE reactor using H_2 carrier gas at 100 mbar. The AlInP(001) epilayers were grown on GaInP(001) buffer layers on n-GaAs(001) substrate with 0.1° miscut toward the [111] direction. After deoxidation of GaAs(001) substrates under tertiarybutylarsine at 620 °C (surface temperature), 100 nm GaAs(001) and 100 nm GaInP(001) buffer layers were grown. Tertiarybutylphosphine (TBP), trimethylindium (TMIn), trimethylgallium (TMGa), and trimethylaluminium (TMAl) were used as precursors. The epitaxially grown layers were doped *n*-type [AlInP(001) $\sim 8 \times 10^{18}$ cm^{-3}; GaInP(001) and GaAs(001) $\sim 1 \times 10^{17}$ cm^{-3}] using ditertiarybutyl silane (DTBSi). The $Al_{0.52}In_{0.48}P(001)$ layer was grown at 100 mbar with a V/III ratio of 60 at 600 °C. To compensate the desorption of P from the AlInP(001) surface during cooling, the TBP precursor was kept open until

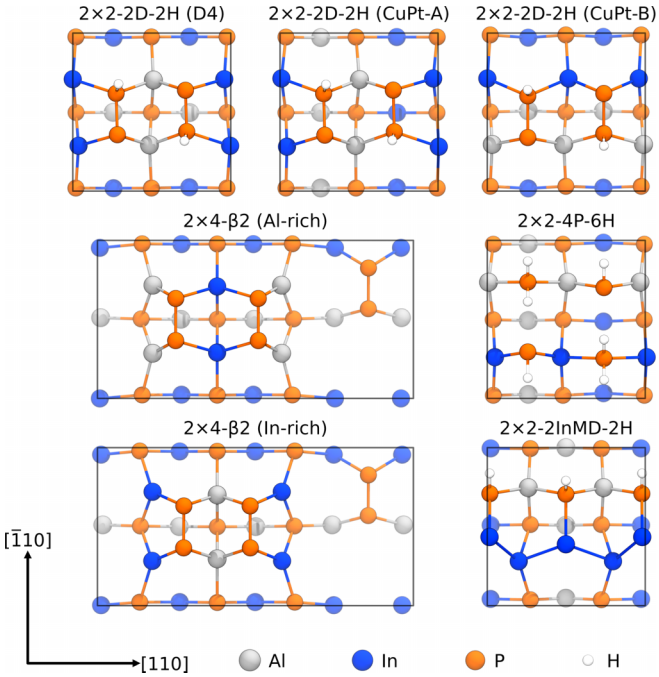

FIG. 1. Top view of energetically favorable clean as well as hydrogenated-terminated $Al_{0.5}In_{0.5}P(001)$ surface structures identified in Refs. [7,8].

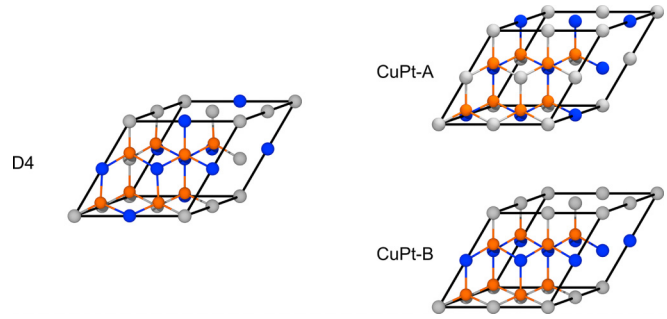

FIG. 2. $Al_{0.5}In_{0.5}P$ bulk material with cations arranged such as to ensure optical isotropy (D4) as well as CuPt-A or CuPt-B ordering. Same color scheme as in Fig. 1.

reaching 300 °C. Subsequently, the TBP precursor was switched off and the sample was annealed for 10 min at 310 °C to remove the excess of P and TBP precursor residuals from the surface. Lattice matching of the AlInP(001) layers to the substrate was confirmed *ex situ* by x-ray diffraction (XRD) in reference samples. In order to investigate the surface reconstruction and chemical composition of the as-prepared AlInP(001) surfaces, selected samples were transferred from the MOVPE reactor in ultrahigh vacuum (UHV) via a dedicated UHV shuttle [25] for low energy electron diffraction (LEED, SPECS ErLEED 100-A) and x-ray photoelectron spectroscopy (XPS, SPECS Focus 500/Phoibos 150/1D-DLD-43-100, monochromated Al-K_α, 1486.74 eV). The entire MOVPE process was observed *in situ* with RAS (Laytec EpiRAS 200), which was set up in such a way that the variation in complex reflection along [011] and [0$\bar{1}$1] was assessed throughout the entire procedure [10]. Afterwards RAS measurements were performed at room temperature. The baseline-correction of the RA spectrum in this work was done using the optically isotropic oxidized Si(100) surface. The calculations are based on density-functional theory (DFT) and performed using the Vienna Ab-initio Simulation Package (VASP) [26]. The general gradient approximation (GGA) using the PBE functional [27] is used to describe the electron exchange and correlation. The electron-ion interaction is described by the projector-augmented wave (PAW) technique [28,29]. The surfaces are modeled using periodic supercells. A vacuum region of about 15 Å is used to decouple the slabs along the surface normal. Slabs with identical reconstructions in both top and bottom layers have necessarily perpendicular dimers and no net optical anisotropy. Therefore, here only the top layer contains the surface reconstruction. The bottom layer is passivated with partially charged hydrogen, $Z = 1.25$ and $Z = 0.75$ for group-III and group-V terminated slabs, respectively. The respective group-III and group-V terminated slabs contain 11 and 12 atomic layers. The electric field in the vacuum region resulting from the two nonequivalent slab surfaces is quenched using a dipole correction [30]. The wave functions are expanded into plane waves up to an energy cutoff of 350 eV. The bulk underneath the surface is modeled with $Al_{0.5}In_{0.5}P$ in such a way as to ensure optical isotropy, using the so-called cubic D4 ordering; see Fig. 2. In addition, we perform calculations where a CuPt-A or CuPt-B ordering is assumed. DFT calculations typically underestimate the band gap due to the inaccurate treatment of the electronic self-energy. On the DFT level of theory we calculate a band gap of 1.26 eV for D4-ordered AlInP bulk, severely underestimating the experimental value of 2.31 eV measured for a random alloy [31]. Using self-consistent *GW* calculations [32], we obtain a value much closer to experiment, 2.25 eV. The small remaining deviation may be partially related to ordering effects: the band gap is expected to be highest in fully disordered alloys [33–35]. For the CuPt-ordered bulk we calculate a band gap of 1.36 and 2.33 eV, with DFT and *GW*, respectively. In addition to self-energy effects, optical spectra are affected as well by local-field and electron-hole attraction effects. They are included here by solving the Bethe-Salpeter equation (BSE) [36–38]. For numerical reasons, we use a model dielectric function in the BSE [39,40] and approximate the *GW* quasiparticle shifts by a scissors operator. This methodology leads to an AlInP bulk dielectric function in very good agreement with the experiment, as shown in Fig. 3. It is used throughout this manuscript, if not stated otherwise.

Following Refs. [11,42–44], the reflectance anisotropy is obtained as

$$\frac{\Delta r}{r}(\omega) = \frac{4\omega}{c}\mathrm{Im}\left[\frac{2\pi\,\Delta\alpha^{hs}(\omega)}{\varepsilon_b(\omega) - 1}\right], \tag{1}$$

where $\varepsilon_b(\omega)$ is the AlInP bulk dielectric function and $\Delta\alpha^{hs}(\omega)$ is the difference of the diagonal tensor elements of the half-slab polarizability corresponding to the respective polarization directions. Following Ref. [44], $\Delta\alpha^{hs}$ is obtained from the dielectric tensor of the slab. This supercell approach necessarily yields not only the surface optical anisotropy, but also contributions from the hydrogen-passivated bottom layer. Fortunately, these contributions are small and occur only for

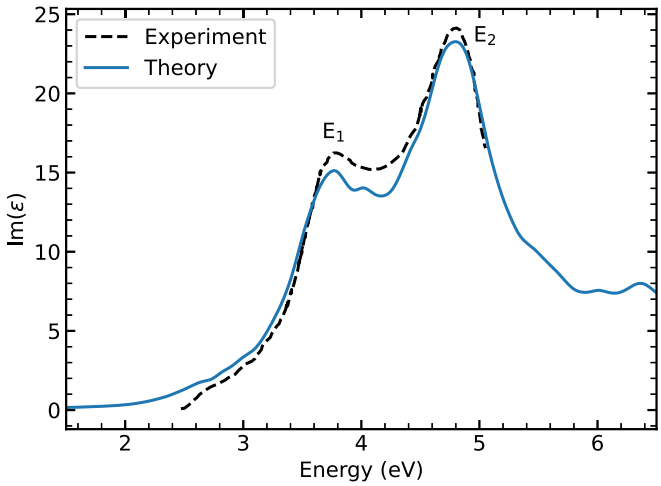

FIG. 3. Imaginary part of the dielectric function of AlInP calculated within the BSE and from experiment [41].

photon energies above 3.5 eV. We get rid of these artifacts by averaging the half-slab polarizabilities for slabs terminated with hydrogen bonds oriented along [110] and [$\bar{1}$10].

III. RESULTS AND DISCUSSION

The RAS spectra measured for epitaxially grown $Al_{0.52}In_{0.48}P(001)$ epilayers at temperatures of 600 °C, 300 °C, and at room temperature are shown topmost in Fig. 4. It is characterized by a negative optical anisotropy for photon energies between 2.1 and 2.8 eV, peaked at around 2.6 eV, and a broad positive feature peaked at around 3.1 eV. A general sharpening of the peaks as well a blueshift is observed for reduced temperatures, similar to the RAS signal of P-rich InP surfaces [45].

Also shown in Fig. 4 are the RAS spectra simulated for the surface structure models shown in Fig. 1. Obviously, the calculated spectra are highly surface specific. This demonstrates that RAS is suitable to discriminate between the various stable AlInP surface structures and may be used for growth monitoring. Among the structures considered here, best agreement with experiment is found for the 2D-2H surface model. It is the only model that reproduces the pronounced negative feature at around 2.6 eV. Given that the 2D-2H surface is also the most dominating structure in the calculated surface phase diagram [8], and that it is consistent with the measured low-energy electron diffraction and x-ray photoelectron spectroscopy data [8], it can be concluded that the AlInP(001) surface produced in the MOVPE environment is composed of a complete layer of phosphorus dimers. Half of the P dangling bonds on the dimers are hydrogen saturated and the other half are filled with lone pairs of electrons.

The pronounced negative RAS feature at 2.6 eV measured here for a MOVPE-grown AlInP(001) surface is reminiscent of earlier observations for InP(001) and GaP(001) surfaces grown by gas-phase epitaxy [46,47]. What is the origin of that peak? In order to answer this question, the surface optical anisotropy due to the transition between single pairs of surfaces states has been calculated on the DFT level of theory. It is found that the most dominant contribution arises from

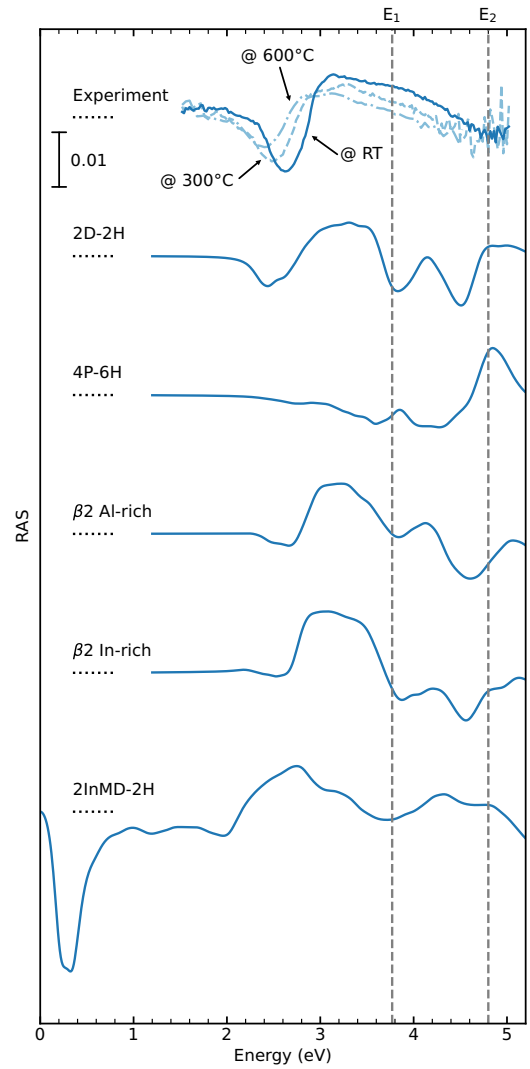

FIG. 4. Comparison of the RAS measurement for spectra of epitaxially grown $Al_{0.52}In_{0.48}P(001)$ epilayers (see text) with calculations for the surface structure models shown in Fig. 1. The 2InMD-2H spectrum is calculated on the DFT level of theory.

direct transitions between the V1 and C2 surface states; see Fig. 5. These states give rise to high joint density of states. The transitions between these states correspond to the excitation of the electrons in the P dangling bonds to antibonding σ^* P dimer states. Thus we can assign the 2.6 eV feature to electronic transitions between electronic states localized at the partially hydrogen-terminated P dimers.

The P dimers of the 2D-2H structure may be arranged differently on the cation sublattice. In order to assess how strongly the local environment influences the RAS fingerprints of these P dimers, three additional structures are considered. They are obtained by rotating and laterally shifting the P monolayer structure on top of the optically isotropic AlInP bulk; see Fig. 6. Two of them, D4-A and D4-B, resemble P dimers on top of a CuPt-A ordered second layer and differ by the dimers forming on top of In or Al atoms on the fourth layer. The third surface, D4-C, results from a rotation of the cation layer by 90°, thus resembling P dimers on top of

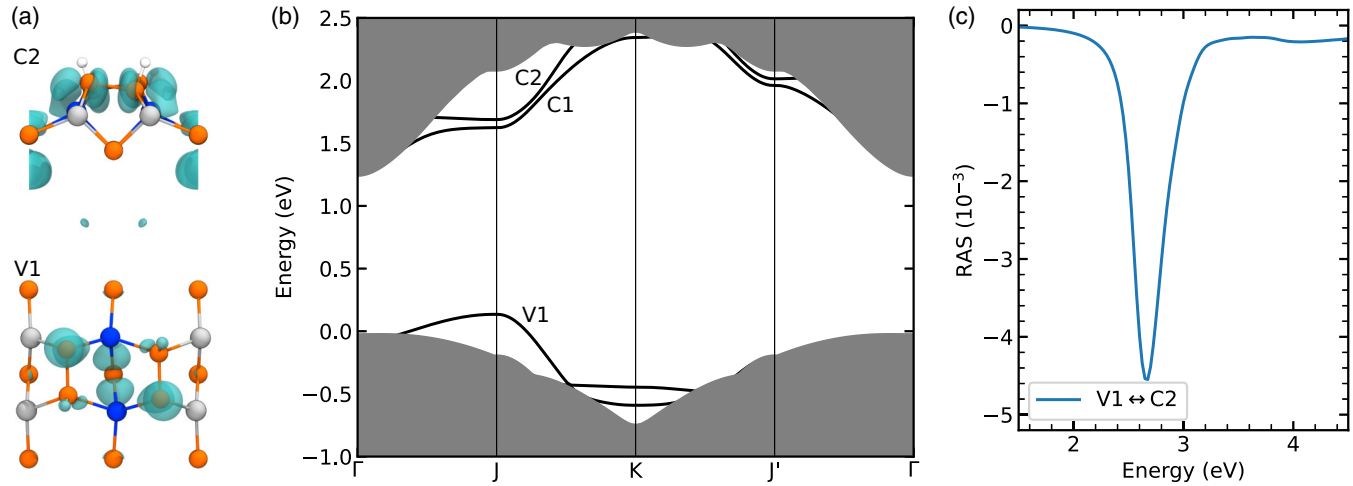

FIG. 5. (a) Orbital character of the prominent surface states V1 and C2. (b) Surface band structure for the (2×2) 2D-2H surface. The gray area is the projected band structure of the bulk. (c) The calculated reflectance anisotropy due to transitions between the V1 and C2 surface states.

a CuPt-B ordered second layer. The RAS spectra calculated for the three model structures are similar to each other and resemble the experimental data, in particular concerning the 2.6 eV feature. This corroborates the finding above, relating this feature to local, intradimer electronic transitions. Notably, the 2.6 eV peak is best reproduced by the D4-B structure, which is energetically most favored due to strain minimization; see also discussion in Ref. [48]. We observe additional negative features near the bulk critical points E_1 and E_2 for all D4 models. Given that the lateral bulk lattice constant has been used for the surface calculations, these features cannot be related to surface-induced strain in the bulk. They need to arise from transitions involving surface modified bulk wave functions. The features differ in magnitude and position for the various D4 models. Therefore, they may partially cancel out in the total signal. This could be an explanation for the absence of pronounced RAS features at the bulk critical points in the measured spectra.

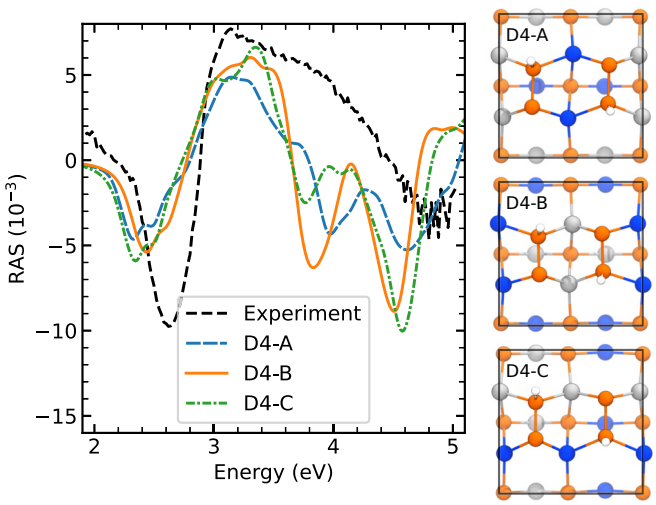

FIG. 6. RAS spectra calculated for different realizations of the 2D-2H model on top of optically isotropic AlInP(001).

While the surface with a 2D-2H reconstruction is stable for a wide range of growth conditions, there occur also other structures in the calculated AlInP(001) surface phase diagram [8]. The 4P-6H surface, see Fig. 1, is stable for very H-rich conditions. It features six hydrogen atoms bonded to the topmost four P atoms in the surface unit cell. The hydrogen termination removes essentially all surface states from the AlInP band gap region. Accordingly, no significant RAS features appear for low photon energies; see Fig. 4. The optical anisotropies at around 3.8 and 4.8 eV coincide with bulk critical point energies and are likely to be related to surface-modified bulk electronic states [49].

The $\beta 2$ surface, known from various binary III-V compounds, is stable for hydrogen-poor conditions. In case of AlInP(001) surfaces, two realizations occur, depending on the cation chemical potential. Both are characterized by occupied surface states around the bulk valence band maximum that are due to antibonding π^* combinations of p_z orbitals localized at the P dimer atoms. Electronic transitions from these dimer states into unoccupied surface resonances as well as transition from occupied surface resonances into empty sp^2 orbitals at threefold coordinated surface cations cause a series of positive RAS features between 2.5 and 4.5 eV; see Fig. 4.

Another very interesting structure is formed for a small range of H-rich and In-rich conditions. It consists of In atomic wires that form along the [110] direction. The band structure of this 2InMD-2H surface features two bands, one occupied, one empty, that strongly disperse in the wire direction, but have nearly no dispersion perpendicular to the wire direction. These two bands are separated by only about 0.3 eV along the $J' - K$ direction of the surface Brillouin zone and pin the Fermi energy at midgap position. Transitions between these two bands give rise to an extremely strong optical anistropy for low photon energies; see Fig. 4. Similar findings are reported for other surface atomic wire systems [50]. The calculations discussed above, performed for various surface structure motifs on top of an optically isotropic AlInP alloy, clearly demonstrate the existence of pronounced RAS features that can be traced to transitions between specific surface states

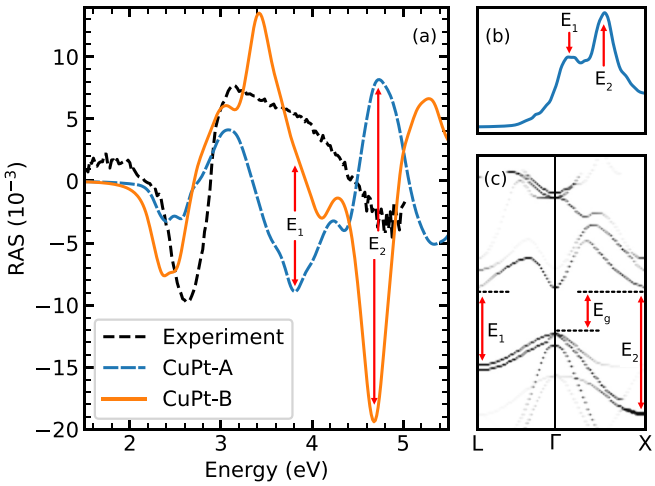

FIG. 7. (a) Measured RAS data in comparison to calculations for the AlInP(001) 2D-2H surface assuming a CuPt-A and CuPt-B type ordering in subsurface layers. (b) Dielectric function calculated for CuPt ordered AlInP, with bulk critical point energies indicated. (c) Calculated AlInP band structure, unfolded according to Ref. [51]. The critical point energies are indicated. E_1 and E_2 are associated with the L and X interband transitions, respectively [52].

and may be used, e.g., for growth monitoring. There are, however, indications that epitaxial growth induces spontaneous CuPt-type ordering on AlInP(001) surfaces [4]. This leads to the questions of how strongly the CuPt ordering does affect the surface RAS signatures and whether RAS can be used to determine the cation ordering in subsurface AlInP layers. In order to answer these questions, calculations were performed for the 2D-2H dimer structure on top of CuPt-A and CuPt-B ordered AlInP(001) subsurface layers. The results are shown in Fig. 7. Obviously, the 2.6 eV anisotropy characteristic for partially H-terminated P dimers is present for both ordering types. This shows that surface structural fingerprints are still present, but may be modified by the ordering in subsurface layers. Strong changes at the RAS signal occur at the E_1 and E_2 critical point energies of AlInP. Here the anisotropy changes sign from negative to positive and positive to negative, respectively, for a transition from CuPt-A to CuPt-B. In fact, this change in ordering is equivalent to rotating the bulk by 90°, while maintaining the orientation of the P dimers. RAS measurements at high photon energies, in particular at the E_2 critical point energy, should thus allow one to determine the degree of order in subsurface AlInP layers. The present experimental setup provides RAS data up to 5 eV. This does not allow for a conclusive statement on the subsurface order. Still, the main experimental features seem slightly better described with the calculations performed assuming CuPt-B type ordering rather than with CuPt-A calculations, even if the sharpness of the measured peaks at energies above 3 eV is not reproduced. This would be in accord with the expectation that [$\bar{1}$11] aligned P dimers induce a CuPt-B type subsurface ordering. We mention that implications of the break of the cubic symmetry on the electronic properties in MOVPE-grown GaInP films have been noted earlier already [53]. The temperature dependence of the GaInP surface signal has been linked to increased bulk ordering as temperature is reduced [18]. For the AlInP surface a similar relation may hold: comparing the signal from the 2D-2H surface on top of isotropic D4 and CuPt-B ordered bulk it can be seen that the main peaks at 2.6 and 3.4 eV are enhanced for the ordered substrate. This also holds for the negative feature at 2.6 eV observed for the $\beta 2$ structure.

IV. SUMMARY AND CONCLUSIONS

Measured RAS data for MOVPE-grown AlInP(001) surfaces are compared with numerical simulations for various energetically favored surface terminations and different subsurface orderings. The results show (i) that different surface structure motifs give rise to clearly distinguishable RAS fingerprints that can be traced to specific electronic transitions. These fingerprints depend only slightly on the local atomic order in the surrounding of the respective structural motif. (ii) The comparison between experiment and theory shows that MOPVE-grown AlInP(001) surfaces are terminated by a monolayer of dimerized P atoms, half of which are hydrogen terminated. (iii) The surface optical anisotropy at high photon energies is strongly modified by the cation ordering in the subsurface layers. In particular, RAS measurements at the AlInP E_2 critical point energy can be expected to allow for conclusions on the degree of CuPt ordering in the material.

ACKNOWLEDGMENTS

Financial support by the Deutsche Forschungsgemeinschaft (PAK981) is gratefully acknowledged. The authors thank the Paderborn Center for Parallel Computing (PC^2) and the Höchstleistungs-Rechenzentrum Stuttgart (HLRS) for grants of high-performance computer time.

[1] C.-W. Kim, G.-Y. Park, J.-C. Shin, and H.-J. Kim, Appl. Sci. **12**, 601 (2022).
[2] D. L. Lepkowski, T. Kasher, J. T. Boyer, D. J. Chmielewski, T. J. Grassman, and S. A. Ringel, IEEE J. Photovoltaics **10**, 758 (2020).
[3] K. Iwata, H. Asahi, T. Ogura, J. Sumino, S. Gonda, A. Ohki, Y. Kawaguchi, and T. Matsuoka, in *Seventh International Conference on Indium Phosphide and Related Materials* (IEEE, New York, 1995), pp. 183–186.
[4] Z. Jinghua, T. Xiaohong, and T. Jinghua, CrystEngComm **11**, 1068 (2009).
[5] W. Yuan and D. C. Hall, J. Appl. Phys. **113**, 103515 (2013).
[6] S. B. Zhang, S. Froyen, and A. Zunger, Appl. Phys. Lett. **67**, 3141 (1995).
[7] I. A. Ruiz Alvarado, M. Karmo, E. Runge, and W. G. Schmidt, ACS Omega **6**, 6297 (2021).
[8] L. J. Glahn, I. A. Ruiz Alvarado, S. Neufeld, M. A. Zare Pour, A. Paszuk, D. Ostheimer, S. Shekarabi, O. Romanyuk, D. C.

Moritz, J. P. Hofmann *et al.*, Phys. Status Solidi B **259**, 2200308 (2022).
[9] D. E. Aspnes and A. A. Studna, Phys. Rev. Lett. **54**, 1956 (1985).
[10] P. Weightman, D. S. Martin, R. J. Cole, and T. Farrell, Rep. Prog. Phys. **68**, 1251 (2005).
[11] W. G. Schmidt, Phys. Status Solidi B **242**, 2751 (2005).
[12] M. M. May, H.-J. Lewerenz, and T. Hannappel, J. Phys. Chem. C **118**, 19032 (2014).
[13] A. Lastras-Martínez, J. Ortega-Gallegos, L. E. Guevara-Macías, O. Nuñez-Olvera, R. E. Balderas-Navarro, L. F. Lastras-Martínez, L. A. Lastras-Montaño, and M. A. Lastras-Montaño, APL Mater. **2**, 032107 (2014).
[14] M. Zorn, J. Jönsson, A. Krost, W. Richter, J.-T. Zettler, K. Ploska, and F. Reinhardt, J. Cryst. Growth **145**, 53 (1994).
[15] K. Haberland, A. Bhattacharya, M. Zorn, M. Weyers, J. T. Zettler, and W. Richter, J. Electron. Mater. **29**, 468 (2000).
[16] C. Krahmer, M. Philippens, M. Schubert, and K. Streubel, J. Cryst. Growth **298**, 18 (2007).
[17] O. Supplie, A. Heinisch, M. Sugiyama, and T. Hannappel, in *2018 IEEE 7th World Conference on Photovoltaic Energy Conversion (WCPEC) (A Joint Conference of 45th IEEE PVSC, 28th PVSEC & 34th EU PVSEC)* (IEEE, Waikoloa Village, HI, 2018), pp. 3923–3926.
[18] M. Zorn, P. Kurpas, A. I. Shkrebtii, B. Junno, A. Bhattacharya, K. Knorr, M. Weyers, L. Samuelson, J. T. Zettler, and W. Richter, Phys. Rev. B **60**, 8185 (1999).
[19] C. Krahmer, M. Philippens, M. Schubert, and K. Streubel, Phys. Status Solidi C **3**, 655 (2006).
[20] A. I. Shkrebtii, N. Esser, W. Richter, W. G. Schmidt, F. Bechstedt, B. O. Fimland, A. Kley, and R. Del Sole, Phys. Rev. Lett. **81**, 721 (1998).
[21] W. G. Schmidt, E. L. Briggs, J. Bernholc, and F. Bechstedt, Phys. Rev. B **59**, 2234 (1999).
[22] N. Esser, W. G. Schmidt, J. Bernholc, A. M. Frisch, P. Vogt, M. Zorn, M. Pristovsek, W. Richter, F. Bechstedt, Th. Hannappel *et al.*, J. Vac. Sci. Technol. B **17**, 1691 (1999).
[23] M. Landmann, E. Rauls, W. G. Schmidt, M. D. Neumann, E. Speiser, and N. Esser, Phys. Rev. B **91**, 035302 (2015).
[24] M. M. May and M. Sprik, New J. Phys. **20**, 033031 (2018).
[25] T. Hannappel, S. Visbeck, L. Töben, and F. Willig, Rev. Sci. Instrum. **75**, 1297 (2004).
[26] G. Kresse and J. Furthmüller, Comput. Mater. Sci. **6**, 15 (1996).
[27] J. P. Perdew, K. Burke, and M. Ernzerhof, Phys. Rev. Lett. **77**, 3865 (1996).
[28] P. E. Blöchl, Phys. Rev. B **50**, 17953 (1994).
[29] G. Kresse and D. Joubert, Phys. Rev. B **59**, 1758 (1999).
[30] J. Neugebauer and M. Scheffler, Phys. Rev. B **46**, 16067 (1992).
[31] J. S. Cheong, J. S. Ng, A. B. Krysa, J. S. L. Ong, and J. P. R. David, J. Phys. D **48**, 405101 (2015).
[32] M. Shishkin, M. Marsman, and G. Kresse, Phys. Rev. Lett. **99**, 246403 (2007).
[33] S.-H. Wei and A. Zunger, Phys. Rev. B **57**, 8983 (1998).
[34] T. M. Christian, D. A. Beaton, K. Mukherjee, K. Alberi, E. A. Fitzgerald, and A. Mascarenhas, J. Appl. Phys. **114**, 074505 (2013).
[35] L. Meier and W. G. Schmidt, Phys. Status Solidi B **259**, 2100462 (2022).
[36] S. Albrecht, L. Reining, R. Del Sole, and G. Onida, Phys. Rev. Lett. **80**, 4510 (1998).
[37] M. Rohlfing and S. G. Louie, Phys. Rev. Lett. **81**, 2312 (1998).
[38] W. G. Schmidt, S. Glutsch, P. H. Hahn, and F. Bechstedt, Phys. Rev. B **67**, 085307 (2003).
[39] F. Bechstedt, R. Del Sole, G. Cappellini, and L. Reining, Solid State Commun. **84**, 765 (1992).
[40] P. Liu, B. Kim, X.-Q. Chen, D. D. Sarma, G. Kresse, and C. Franchini, Phys. Rev. Mater. **2**, 075003 (2018).
[41] E. Ochoa-Martínez, L. Barrutia, M. Ochoa, E. Barrigón, I. García, I. Rey-Stolle, C. Algora, P. Basa, G. Kronome, and M. Gabás, Sol. Energy Mater. Sol. Cells **174**, 388 (2018).
[42] R. del Sole, Solid State Commun. **37**, 537 (1981).
[43] R. Del Sole and E. Fiorino, Phys. Rev. B **29**, 4631 (1984).
[44] F. Manghi, R. Del Sole, A. Selloni, and E. Molinari, Phys. Rev. B **41**, 9935 (1990).
[45] S. Visbeck, T. Hannappel, M. Zorn, J.-T. Zettler, and F. Willig, Phys. Rev. B **63**, 245303 (2001).
[46] W. G. Schmidt, P. H. Hahn, F. Bechstedt, N. Esser, P. Vogt, A. Wange, and W. Richter, Phys. Rev. Lett. **90**, 126101 (2003).
[47] P. H. Hahn, W. G. Schmidt, F. Bechstedt, O. Pulci, and R. Del Sole, Phys. Rev. B **68**, 033311 (2003).
[48] J. E. Bernard, S. Froyen, and A. Zunger, Phys. Rev. B **44**, 11178 (1991).
[49] W. G. Schmidt and J. Bernholc, Phys. Rev. B **61**, 7604 (2000).
[50] S. Chandola, K. Hinrichs, M. Gensch, N. Esser, S. Wippermann, W. G. Schmidt, F. Bechstedt, K. Fleischer, and J. F. McGilp, Phys. Rev. Lett. **102**, 226805 (2009).
[51] P. V. C. Medeiros, S. Stafström, and J. Björk, Phys. Rev. B **89**, 041407(R) (2014).
[52] T. Kim, S. Hwang, J. Byun, D. Aspnes, E. Lee, J. Song, C.-T. Liang, Y.-C. Chang, H. Park, J. Choi *et al.*, Current Appl. Phys. **14**, 1273 (2014).
[53] A. Mascarenhas, S. Kurtz, A. Kibbler, and J. M. Olson, Phys. Rev. Lett. **63**, 2108 (1989).